KSME

Springer

Journal of Mechanical Science and Technology 34 (10) 2020

Original Article
DOI 10.1007/s12206-020-0907-8

Keywords:
· Punch strength simulation
· Punch stress distribution
· Additive manufacturing (AM)
· Semi-AM punch
· Semi-AM range
· Semi-AM shape design
· Semi-AM shape verification
· Feasibility verification

Correspondence to:
Soon-Yong Yang
soonyy@ulsan.ac.kr

Citation:
Zhang, G., Wang, S., Kim, Y.-S., Choi, S.-W., Yum, Y.-J., Yang, S.-Y. (2020). The design of a semi-additive manufacturing shape using metal 3D printing for a partially strengthened mold based on a high-alloy tool steel powder. Journal of Mechanical Science and Technology 34 (10) (2020) 4149~4159.
http://doi.org/10.1007/s12206-020-0907-8

Received March 8th, 2020
Revised June 10th, 2020
Accepted August 4th, 2020

† Recommended by Editor
Chongdu Cho

The design of a semi-additive manufacturing shape using metal 3D printing for a partially strengthened mold based on a high-alloy tool steel powder

Gaoqi Zhang[1], Shiliang Wang[1], Yong-Seok Kim[1], Seong-Woong Choi[2], Young-Jin Yum[1] and Soon-Yong Yang[1]

[1]Department of Mechanical Engineering, University of Ulsan, Ulsan 44610, Korea, [2]Department of Construction Machinery Engineering, University of Ulsan, Ulsan 44610, Korea

Abstract In this paper, describe the fabrication of high strength punch molds that can be applied to ultra-high strength sheet materials after processing. A method for improving the strength of the punching die by additive manufacturing (AM) of a high strength powder material using a metal 3D printer was proposed. Furthermore, a semi-additive technique was proposed to increase the punch strength through partial AM of specific parts of the punch that require high strength. A preprocessing process for predicting the semi-additive shape for the punch function portion is proposed for application of the AM technology of a metal 3D printer to this semi-additive technique. The preprocessing for determining the semi-additive shape consists of the predicting step of the punch strength based on the shear process of the sheet material, analyzing step the stress distribution of the punch, defining step the semi-additive range, designing step the semi-additive shape, and verifying step the additive interface strength. Based on this simulation, the range of shapes for the semi-additive was 1.21 mm and 2.62 mm for sheet material CP1180 and 1.3 mm and 3.2 mm for sheet material 22MnB5. The shape and range determined in the simulation process defines a semi-additive area (volume) for the 3D printing AM technique using a high-strength powder material, and a semi-additive punch was manufactured according to the defined area. The semi-additive punch (HWS powder material) fabricated in this study was performed a durability test for validity verification in the piercing process of high-strength sheet material (CR980). This validation test compared the state of the punch after 1000 piercing processes with a typical cold piercing punch (SKD11 solid material). From this test, the feasibility of the semi-additive punch was confirmed by showing a similar state of scratches and abrasion from the two punches. The simulation analysis processor for the additive shape and the additive range prediction for the semi-additive punch manufacturing presented in this paper can be useful for the additive manufacture of cutting and trimming punch mold.

1. Introduction

The automotive sector is in need of lighter and stronger materials. One technical approach is hot stamping molding; though technically preferred, there are difficulties in post-processing (piercing or trimming process), cost, time and space of this technique because the post-processing is mostly performed by a laser process. Many efforts have been made to convert these laser processes into press processes at the production site. However, a press process that requires a strengthened post-processing mold has not yet been achieved due to technical limitations. The transition from the laser process to the press process to improve the hot stamping. must be accompanied by a more advanced mold strengthening technology. The parts with increased strength due to the hot stamping can easily damage the mold due to strong reaction forces, thus reducing the surface quality and dimensional accuracy of the product and reducing

the life of the mold [1, 2]. Damage of the shear punch mold in the press process can include chipping, cracking, gross fracture, and galling. Such damage is caused by mismatch of the hardness, toughness, and abrasion resistance of the mold material. A method for heat treatment and nitriding the surface of a punch mold and then performing a surface treatment (coating) or a heat treatment to generate another surface layer element is usually used to solve such problems. Surface treatments are not a fundamental solution because deeper coatings require a higher cost, and deep, strong heat treatments increase the probability of chipping. Although mold strengthening technologies include a variety of classical techniques, recently, studies in the mold strengthening field introduced the metal 3D printing technology [3-5]. Many studies have investigated metal mold manufacturing and mold strengthening using in a cold press forming process with the metal 3D printing direct energy deposition (DED) technology. Furthermore, studies using high-alloy tool steel powders have used surface hardening to improve high-strength molds and mold performance [6-9]. High-speed steels (in high-alloy tool steels) are some of the most interesting tool steels because the various alloying elements (Mo, V, W, etc.) in the material enhance the hardness and wear resistance. However, high speed tool steel has the advantage of having excellent performance but is vulnerable to brittle cracking because of its high carbon content. Many researchers have attempted various studies to overcome the weakness of brittle cracks in the additive manufacturing (AM) process. Nevertheless, there is still no report of technically perfect parts made by full-additive manufacturing with high-alloy tool steels.

In this study, a semi-additive manufacture technique was proposed for the AM of only the part requiring high strength to minimize the AM range (additive thickness and volume capacity) as a method to compensate for the weak points (brittle crack) of using metal 3D printing AM technology in the mold field. In this study, the punch strength prediction simulation and stress distribution analysis of the sheet material piercing process were performed to apply the semi-AM technique [10]. A study was conducted to select a semi-AM range from the stress distribution of the punches [11]. Additionally, the semi-additive shape was designed [12] according to the predicted semi-AM range, and verification analysis of the designed semi-additive shape and interface portion of the punch body was performed [13]. The effectiveness of the semi-AM technique simulation was verified through the fabrication and durability testing of the piercing additive punch based on the additive shape and additive range selected from the simulation results.

2. Punch strength prediction processor and mechanical properties of the materials

This study was performed to predict the punch strength required for shearing (piercing) of high strength CP1180 (1200 MPa) and 22MnB5 (1500 MPa) parts. Additionally, this study was designed to identify the stress distribution that concentrates on the punches and to use it for partial AM (semi-additive) by 3D printing. In other words, the method predicts the width and depth of the punch where the stress is concentrated, selects the punch shape range that actually affects the shear action of the punch, and partially increases the punch strength. An analytical simulation for predicting the punch strength was performed based on the high strength sheet piercing process variables. The conditions and ranges for the piercing process analysis were selected based on previous research on the shear mechanism and process analysis of sheet materials. The simulation processor for the punch strength required for the high-strength parts piercing process introduced in this study is shown in Fig. 1. The tensile strength of the sheet material for this process analysis was selected as a material with a 1200 MPa (CP1180: Complex Phase Steel) and 1500 MPa (22MnB5: Boron Steel). The thickness of the sheet material was 1.2 mm. The punch materials were the cold work material SKD11 (substrate material), high wear resistance steel (HWS, additive material), and M4 (additive material), which is a high-speed tool steel. The mechanical properties of the punch and sheet materials for this process analysis were selected from the literature analysis and the mechanical property test, as shown in Table 1. In general, the mechanical properties of the material differ depending on the source, indicating the material must be tested and simulated simultaneously for accurate analysis. The simulation software for the piercing process analysis used the

Table 1. Mechanical properties of the sheet and punch materials for analysis simulation (S: Sheet, P: Punch).

Material	CP1180(S)	22MnB5(S)	SKD11(P)	HWS(P)	M4(P)
YM (GPa)	210.0	212.0	207.0	198.0	214.0
YS (MPa)	951.51	1010.0	-	2303.0	-
TS (MPa)	1241.99	1500.0	2181.0	2715.0	-
PR	-	-	0.29	0.298	0.3
CDV	1.1(cold)	2.28(hot) 0.48(cold)	-	-	-
Ref.	[16-18]	[19-24]	Experiment	Experiment	MatWeb

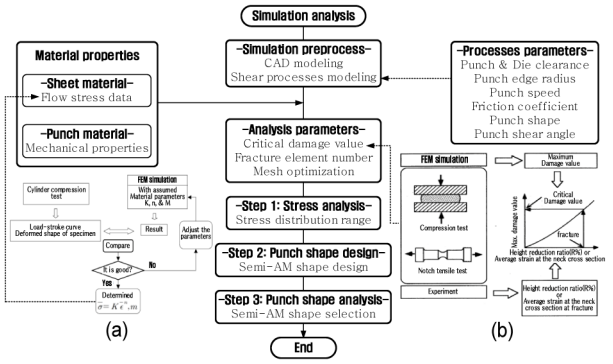

Fig. 1. Simulation processor for punch strength prediction: (a) interpolation of flow stress data [14]; (b) calculation of the critical damage value [15].

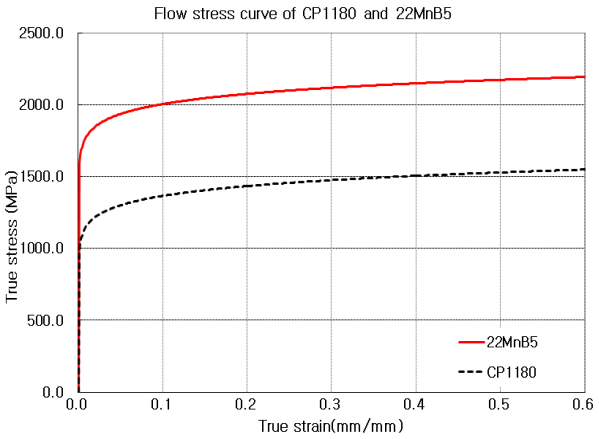

Fig. 2. Flow stress curve of sheet material CP1180 and 22MnB5.

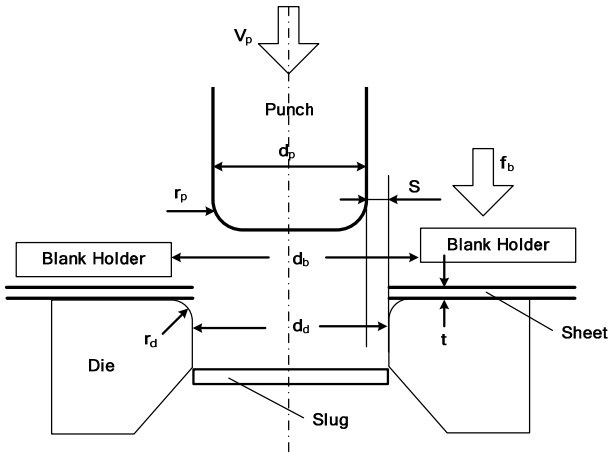

Fig. 3. Main parameters and conceptual schematic for the piercing process analysis.

DEFORM 2D code, which implements the processes of shearing and propagating the material geometrically such that it is similar to a real-world scenario. As an implementation method for the shearing process, when the fracture critical value at which the fracture occurs in the material is reached, the elements of the sheared portion are deleted. This requires knowing the number of erasure elements required for visual processing and the ductile fracture value at which shear (fracture) occurs, which is a characteristic of the material. To realize a precise shearing mechanism close to the actual mechanisms, it is necessary to generate a dense mesh in the shear portion, and a high level of software expertise is required. Previous studies have shown that these values (number of erasure elements, ductile fracture value, mesh density) are difficult to generalize depending on the material and are determined by experimental values and repeated analytical values. Therefore, optimization of these values requires a process of finding the value by comparing the experimental and simulation values based on the target material and repeating the analysis [15].

However, in the present study, the fracture critical value (critical damage value) for the high-strength sheet materials was selected from Refs. [25, 26]. The fracture thresholds based on the ductile failure theory (Cockcroft and Latham) for sheet materials CP1180 and 22MnB5 were 1.1 (cold work) and 0.48 (cold work)/2.28 (hot work), respectively. In addition, the DEFORM code uses plastic flow data as the basis of the simulation, so that the flow stress curve data for the target sheet material are necessary. The flow stress data can be collected from a variety of sources, but are provided only as a reference, so material testing is essential to obtain data for specific application fields. In addition, to apply this test data to the simulation, the s-s curve data from the test must be compensated [14]. In this paper, the flow stress curves for sheet materials were analyzed and selected from Refs. [16, 25, 26]. The Hollomon models of the flow stress data curves for the selected sheet materials CP1180 and 22MnB5 were $\bar{\sigma} = 1605.\varepsilon^{0.07}$ and $\bar{\sigma} = 2178.2.\varepsilon^{0.103}$, respectively and the data curves are shown in Fig. 2.

3. Main parameters for piercing process analysis

A two-dimensional plane strain model was used for the piercing process analysis and the conceptual parameter schematic are shown in Fig. 3. The process parameters affecting the results of the piercing analysis are sheet material thickness, punch diameter, punch corner radius, holder diameter, die diameter, stripper force, punch speed, friction coefficient, and punch and die clearance. The clearance between punch and die is the main process parameter. Industry long experience in clearance between punch and die suggests that 5 % of the sheet material side thickness is standard. However, the clearance is determined by the thickness of the sheet material, the

tensile strength, the material type and the requirements of a specific operation. In this study, the process parameters were analyzed and selected from literature based on the shear analysis of high-strength sheet materials [16, 27]. The clearance for the high-strength sheet material CP1180 is 10-18 % the sheet thickness, a punch speed of 50 mm/sec, and a punch corner radius of 0.005-0.03 mm.

The optimum process parameters required for the punch strength prediction simulation were selected from the results of this piercing process analysis, as summarized in Table 2. In addition, based on the simulation analysis processor and selected piercing process parameters presented in this study, the prediction simulation of the punch strength required for the piercing shearing process of the high strength CP1180 and 22MnB5 sheet material was performed.

4. Prediction simulation for the punch strength and semi-additive range

The analytical model for the punch strength prediction simulation is shown in Fig. 4. Fig. 4(a) shows a two-dimensional plane strain model for punch strength prediction simulation, and Fig. 4(b) represents the elastic (punch) and plastic (sheet)

Table 2. Process parameters for the prediction simulation of punch strength.

Parameter		Value
Sheet material	Material	CP1180 / 22MnB5
	Thickness ' t '	1.2 mm
	Flow stress curve data (MPa)	$\bar{\sigma} = 1605.\varepsilon^{0.07}$ $\bar{\sigma} = 2178.2.\varepsilon^{0.103}$
	Fracture critical value	1.1(cold) / 2.28(hot), 0.48(cold)
Punch diameter ' d_p '		10.0 mm
Punch corner radius ' r_p '		0.01-0.02 mm
Stripper diameter ' d_b '		10.06 mm
Die diameter ' d_d '		10.12 mm ($d_p + s$)
Die corner radius ' r_d '		0.01-0.02 mm
Stripper pressure (' f_b '/area)		Various conditions MPa
Punch and die material		SKD11 / HWS / M4
Punch velocity ' V_p '		50 mm/sec
Coefficient of friction		0.12 shear friction
Punch & die clearance 'S'		0.005-0.24 mm (2 %t-20 %t)

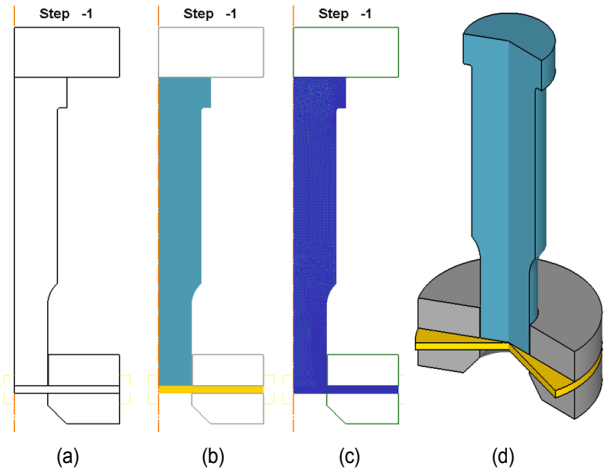

Fig. 4. An analysis model for the prediction simulation of the punch strength.

bodies at which deformation occurs in the analysis process. Fig. 4(c) shows the finite element model for analysis and Fig. 4(d) is the CAD model showing the three-dimensional representation of the 2D analysis model.

The state of the progress step in the punch strength prediction simulation is shown in Fig. 5. Figs. 5(a) and (b) are 2D finite analytical models showing the generation of dense elements (meshes) in regions where the shear phenomenon of the sheet material and the occurrence of concentrated stress in the punches are expected. The generation of dense elements (meshes) in these areas of interest can have more accurate analysis results and analysis (shear mechanism) phenomena. Fig. 5(c) shows a state in which shearing begins in the sheet material, while Fig. 5(d) shows a state in which shearing is

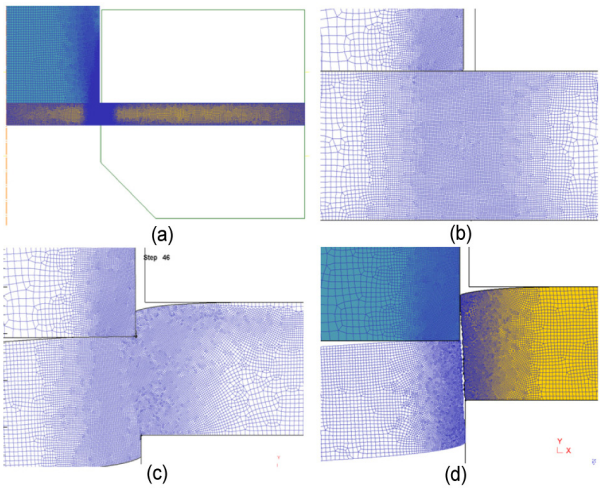

Fig. 5. The state of each progress step in the punch strength prediction simulation.

completed. Based on the punch strength analysis, the AM range (shape and size or area and volume) is determined by analyzing the maximum stress distribution of the punch.

4.1 Punch die clearance and punch stress

An analytical method and the simulation results of the punch strength predictions are shown in Fig. 6 and Table 3, respectively. The punch strength prediction simulation was performed according to the clearance between the punch and die, and the radius of the punch blade edge. Fig. 6(a) shows the maximum stress distribution in the blade of the punch, and Fig. 6(b) shows a state in which a large stress is generated on the side surface of the punch in the shearing process. Fig. 6(c) shows the punch load change according to the punch stroke, and Fig. 6(d) shows the contour line of the stress distribution when the maximum stress occurs in the punch. Table 3 summarizes the depth (Ld) and height (Lh) of the punch shape based on the contour line (Fig. 6(d)) of the stress distribution when the maximum stress occurs in the punch. A graph of the maximum stress and stress distribution range from the simulation result data of the punch strength prediction for the high-strength sheet material (CP1180) is shown in Fig. 7. Figs. 7(a) and (b) show the clearance of the punch and die, and the depth and height of the punch shape based on the punch corner radius, respectively. Figs. 7(c) and (d) show the clearance of the punch and die, and the maximum stress and maximum stress generating stroke based on the punch corner radius, respectively. In the piercing process, the maximum stress and shape range of the concentrated stress acting on the punch was independent of the punch corner radius and punch die clearance. However, the stroke (S) where the maximum stress occurs was greatly affected by the punch corner radius (R) (S = 0.096 mm when R = 0.01 mm, S = 0.2394 mm when R = 0.02 mm).

The average maximum stress acting on the punches in the piercing process of the high strength sheet material CP1180

Table 3. Simulation results for the punch strength predictions.

Punch & die clearance (t × [%])	Punch concentration stress distribution				Punch maximum stress [MPa]	
	Depth (L_d) [mm]		Height (L_h) [mm]			
	R = 0.01	R = 0.02	R = 0.01	R = 0.02	R = 0.01	R = 0.02
2 %	1.05	1.25	2.55	2.65	2270	2200
3 %	1.30	1.45	2.65	2.95	2210	2130
5 %	1.00	1.25	2.65	2.65	2230	2260
7 %	1.20	1.25	2.50	2.75	2290	2220
8 %	1.25	1.15	2.75	2.55	2240	2330
10 %	1.25	1.05	2.70	2.50	2230	2300
13 %	1.25	1.25	2.65	2.65	2270	2250
17 %	1.30	1.10	2.60	2.45	2240	2380
20 %	1.25	1.10	2.65	2.40	2220	2340
Average	1.21	1.21	2.63	2.62	2244	2268

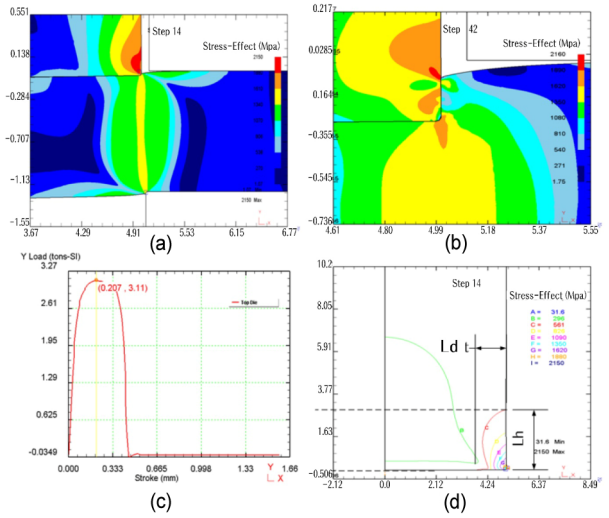

Fig. 6. Analytical method of the simulation results for punch strength prediction.

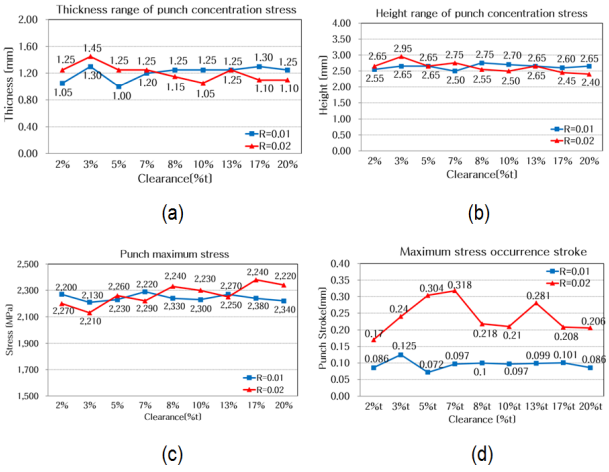

Fig. 7. Maximum stress and stress distribution based on the simulation result data.

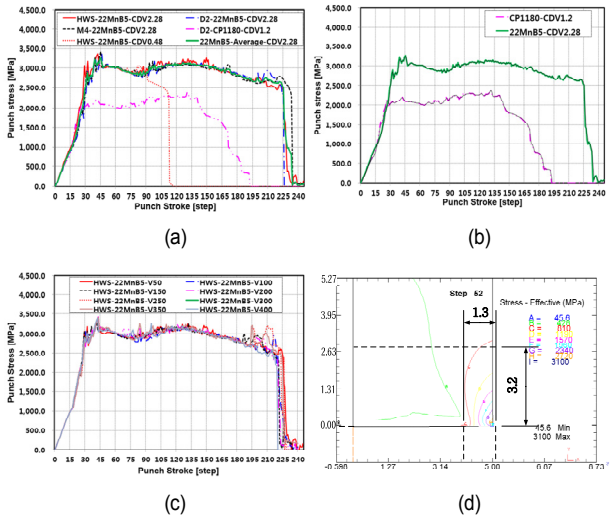

Fig. 8. The punch strength simulation according to the punch speed, punch materials and sheet materials.

was 2256 MPa, and the depth and height of the punches with intensive stress were 1.21 mm and 2.625 mm, respectively.

4.2 Punch speed and punch stress

This simulation was carried out to observe the punch strength according to the punch speed, punch material and sheet material. Fig. 8(a) shows the punch stress based on the punch material and sheet material, and Fig. 8(b) shows the punch stress distribution based on the punch speed for punch material HWS and sheet material 22MnB5. Fig. 8(c) shows the stress of the punch according to the sheet material, and Fig. 8(d) shows the range of the stress distribution acting on the punch when the sheet material is 22MnB5. As shown in Fig. 8(a), the punch stress was barely influenced by the punch materials (HWS, M4, D2) and was dominantly affected by the sheet material (CP1180, 22MnB5). Additionally, the critical damage value (CDV) was not influenced in the punch stress but affected the shearing time point of the sheet material. As shown in Fig. 8(b), the unstable change in stress values at the time point when the punch stress drops sharply (Step 185-225) is a phenomenon that occurs in the shearing process. The irregularities of the remeshing time point in the software, and the difference in the mesh density that changes in every remeshing steps acts as an instability factor of the shear. Therefore, it is not necessary to give a specific meaning to this phenomenon. In addition, the phenomenon in which the punch stress sharply increased, partially in the shearing process, is that the sheared sheet material is pressed by the minute region of the punch side. This causes the side surface of the punch to wear and scratch in the actual piercing process. As shown in Fig. 8(c), the punch speed (50-400 mm/sec) in the piercing process did not appear to affect the change of the punch stress. The punching speed does not affect the punch stress significantly if the punching speed is not very slow and the speed is

faster than a certain level (50 mm/sec). Fig. 8(d) shows the distribution contours of the punch stress generated in the shear process for the 22MnB5 sheet material, and the depth and width of the stress acting were analyzed as 1.3 mm and 3.2 mm, respectively. At this time, the maximum stress of the punch was 3267 MPa. The range of the semi-AM shapes can be determined from the punch stress distribution according to the punch and die clearance, and the punch speed and the punch stress distribution according to the sheet material. Based on this simulation, the range of shapes for the semi-additive was 1.21 mm and 2.62 mm for sheet material CP1180 and 1.3 mm and 3.2 mm for sheet material 22MnB5.

5. Semi-additive shape design

An analytical simulation was performed to predict the punch strength distribution required for the piercing process for high-strength sheet materials. Then, the stress contours appearing along the punch strength distribution were analyzed to measure the depth (Ld)) and height (Lh)) of the punch shape range. From the measured punch shape range, a semi-additive area was defined, and, the shape of the punch blade portion for the semi-additive was designed as shown in Fig. 9. Fig. 9(a) shows an example of a piercing punch body shape for a semi-AM, and Fig. 9(b) shows the dimensional definition of a punch blade shape. Fig. 9(c) shows variously designed semi-additive shapes of the punch blade portion.

The friction coefficients generated at the interface between the punch body material and semi-additive material as a preliminary simulation for the strength analysis of each semi-additive shape were derived through trial and error. This was also used to analyze the characteristics of the simulation software and verify the characteristics of the analysis software in advance of the analysis of the semi-additive shapes. The interface boundary conditions for this analysis software are classified into shear (sticking), coulomb (sliding), hybrid, and tau frictions. Here, the shear and coulomb friction conditions provide information on the separation and slip at the bond interface boundary in the analysis process, and tau friction conditions provide shear stress information at the bond interface. In addition, a hybrid friction condition means that the shear and coulomb conditions are applied at the same time, which can simultaneously observe the state of the separation and slip at the bond interface boundary. Therefore, this analysis was performed to determine the friction type and friction coefficient to be used as a reference. This analysis method is proposed based on the fact that the change of stick, slip, separation, and other factors occur at the interface of the heterogeneous materials depending on the friction conditions that affect the damage value of shear materials. This method was applied to observe the bond strength at the deposited interface between the punch body and powder material. Some of the simulation results performed according to the method (friction type and friction coefficient) presented above are shown in Fig. 10, determining the characteristics of the simulation software. Fig. 10(a) shows a

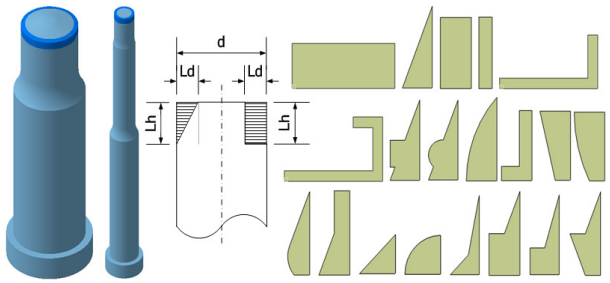

Fig. 9. Designed punch blade shape and shape range for the semi-AM.

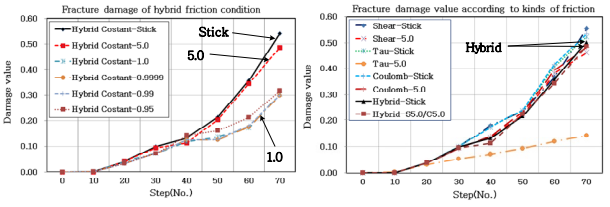

Fig. 10. Comparison of fracture damage for various kinds of contact surface friction conditions: fracture damage of the (a) hybrid friction condition; (b) various kinds of friction.

comparison of the fracture damage values based on the size of the hybrid friction condition, and Fig. 10(b) shows values according to the kinds of friction conditions. Descriptions of this simulation are omitted because we could not find a significant trend based on the software due to variations in the friction coefficient in shear friction, coulomb friction, and tau friction conditions. As shown in Fig. 10(a), an important finding here is that the change in the value of damage caused by the adjustment of the friction coefficient tends to be significant in the hybrid friction conditions compared to other friction conditions. In addition, the magnitude of the friction coefficient presented as a condition is conceptually different from the friction coefficient applied as a condition in a general molding operation, and is an exceptional value found by trial and error. As shown in Fig. 10(b), the fracture damage values according to the frictional conditions show a similar tendency in all conditions except the tau condition. However, only the hybrid friction condition shows a clear difference when the magnitude of the friction coefficient is 1.0 and 5.0. Specifically, the hybrid friction condition means that the boundary condition can be controlled at the joint surface according to the user's definition. Therefore, the frictional condition of the process analysis for the simulation finding the best shape in the semi-additive shape to strengthen the blade portion of the piercing punch was selected to be 5.0 for the hybrid-type friction coefficient (shear and coulomb).

6. Semi-additive shape simulation and results

The simulation analysis for the selection of the semi-additive shape was performed based on the friction conditions of the

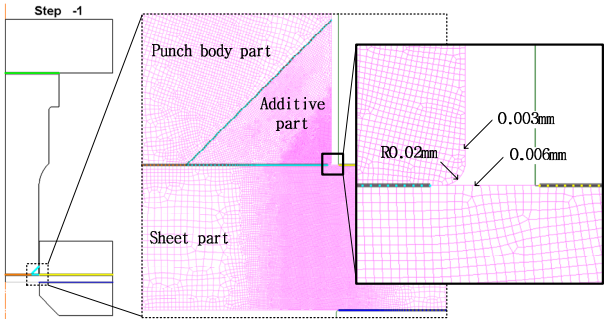

Fig. 11. Simulation analysis model: (a) contact boundary condition; (b) mesh element state and size.

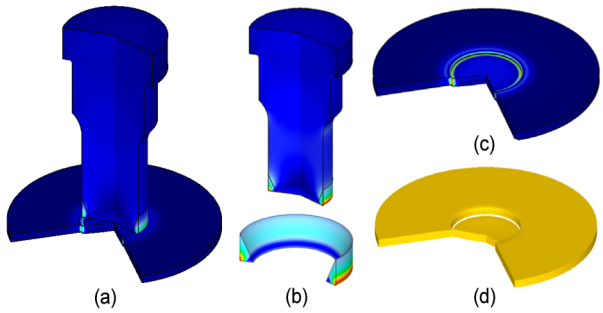

Fig. 12. Simulation results: (a)-(b) stress distribution of the semi-additive punch; (c) stress distribution of the shear sheet material; (d) shea shape of sheet material.

heterogeneous material interface obtained through the piercing process analysis condition and software characteristics analysis mentioned above. The simulation model of the semi-additive shape is shown in Fig. 11. Fig. 11(a) shows the simulation analysis model and the contact condition between the interface boundary for the semi-additive shape, and Fig. 11(b) shows the state and size of the meshed simulation analysis object. In particular, the generated mesh was very dense in the semi-additive edge portion where stress is concentrated and in the sheet material portion where shear occurs. The analytical shape and stress distribution of the simulation results performed for the optimal shape selection in the semi-additive shapes is shown in Figs. 12 and 13, respectively. Fig. 12(a) shows the case of the plate type showing the most stable state among the semi-additive shapes in which the simulation was performed. Fig. 12(b) shows the case of the equilateral triangle type, which is relatively unstable due to separation at the junction boundary. Figs. 12(c) and (d) show the stress distribution and shear state of the sheared sheet material, respectively. A comparative example of the stress distribution between the case of the stable state and the poor stability among the semi-additive shapes is presented in Fig. 13. Fig. 13(a) shows the flat-type stress contour showing the most stable state among the simulated semi-additive shapes and shows that the stress contours progress smoothly from the sheet material through the semi-additive region to the punch body.

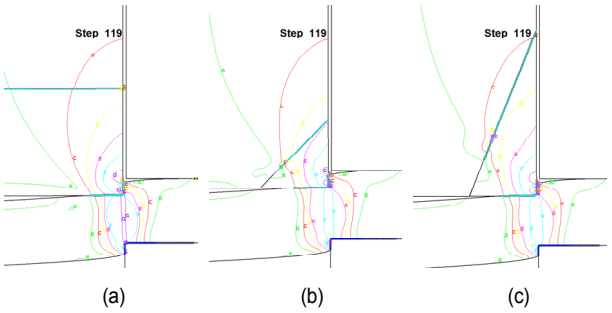

Fig. 13. Simulation results: stress distribution contour of the (a) plate; (b) equilateral triangle; (c) right triangle shape types.

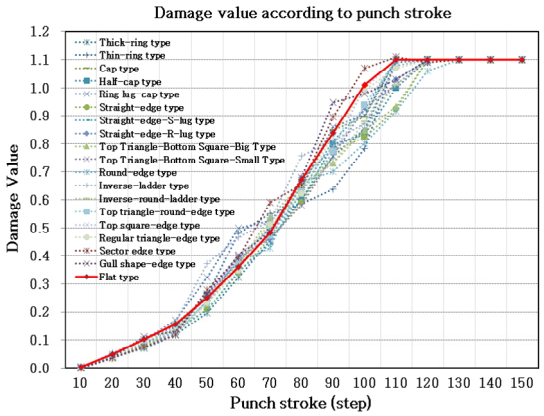

Fig. 14. Comparison of the sheet material damage values for semi-additive shapes.

However, Figs. 13(b) and (c) show the stress contours in the case of a triangular section with relatively low stability due to separation at the bond interface boundary, which indicates that stress contours do not progress smoothly at the bond interface boundary. In this semi-additive shape simulation analysis, the maximum stress occurred at the time point initiation (stroke-Step 119) of shearing at the sheet material. In the simulation analysis for this semi-additive shape selection, the stability at the bond interface was indirectly judged by comparing the damage value acting on the sheet material based on the designed semi-additive geometry.

Another criterion comprehensively considered the range of the stress distribution, slip and separate state at the interface, the size of the additive range, and the degree of difficulty for the additive manufacturing. Based on the simulation results for each semi-additive geometry, a comparative graph of the damage values is shown in Fig. 14. In addition, the cases of slip and separation at the bond interface are shown in Fig. 15. Based on this analysis, the most stable shape was determined to be the plate type. This is because the change of the damage value was observed very stably compared to other shapes, as shown in Fig. 14. Alternatively, the change trend of the damage value in other shapes is observed irregularly. This seems to affect the damage value at every moment by influencing the slip, separating and bending moment depending on the ge-

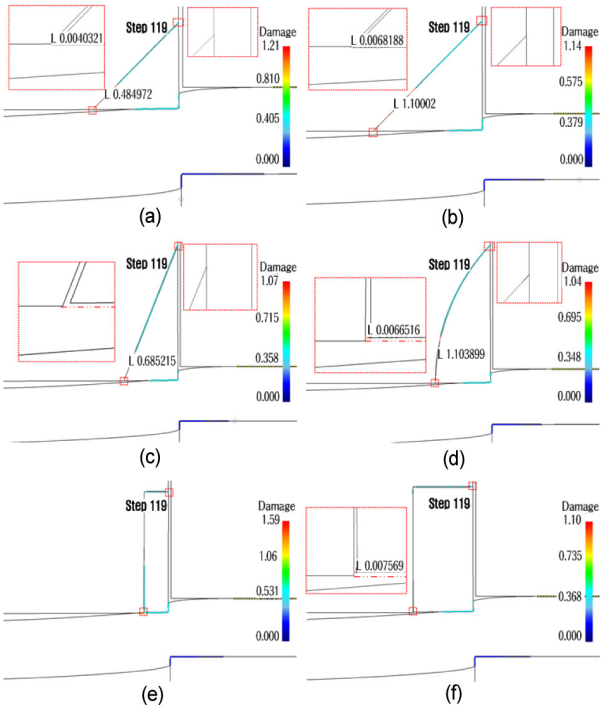

Fig. 15. Description of the stability at the interface according to the semi-additive geometry.

ometry and size of the interface boundary. Here, the large increase of the damage value at the small punch stroke is analyzed given the separating or bending moment at the edge pointer where the contact starts to be geometrical. Additionally, despite the large strokes that can cause shearing, the failure to reach the critical damage value of the shear is analyzed as the effect of the slip at the bond interface. The plate-type shape was the most stable, followed by the wedge shape with a triangular cross section. In addition, the triangular cross section was more stable when the bond interface had a 45 degree rather than a vertically or acute-angle shape. An example explaining the stability from the simulation results is summarized in Fig. 15. Figs. 15(a) and (b) show that in the case of an equilateral triangular cross sections with a 45-degree interface, the size of the cross section does not affect the slip but rather the degree of separation. Fig. 15(c) shows that the case of a scalene triangle cross section with an acute angle interface is easier to cause slip than an isosceles triangle section. Fig. 15(d) shows a case where the interface is curved, which was vulnerable to both separation and slip. Therefore, the case where the cross section has an isosceles triangle section is more stable than an acute triangle section.

Additionally, the interface consisting of pure straight lines is more stable than when the interface includes a curve. Figs. 15(e) and (f) show a ring type of a rectangular cross section with a vertical interface, the greater the separating (opening) appears as the interface moves away from the punch blade, and slip does not occur. However, the phenomenon in which the additive portion is contracted by compression and a step is generated between the punch body and the additive part appears. Therefore, in the ring-shaped additive shape, AM as thin as possible in the depth direction of the punch body is advantageous for reducing separation.

7. Discussion

The most stable semi-additive shape was a simple flat type, and no slip or separating phenomenon appeared at the additive interface. The stress distribution shows nearly the same tendency as in the punch of a solid material because the shearing force of the punch is transmitted stably to the sheet material. Additionally, separating, slip, and bending due to the moment occurs easily at the additive interface consisting of vertical or diagonal lines in the semi-additive shapes. Moreover, separation occurred in the shape with an interface close to the vertical, and the slip was more affected as the angle inclined diagonally to the acute angle. Therefore, in the present semi-additive punch, the formation of the additive interface in the same direction as the direction in which the punching force is applied should be avoided. Specifically, the AM direction is preferably deposited in the vertical plane direction to which the punch load is applied. As in the present study, the design of the partially semi-additive shape for punch strengthening is aimed at minimizing the additive time and reducing the additive volume for the cost of high strength powder. Moreover, since there is a limit to the additive range of the high-strength tool steel (high speed steel) powder, the purpose of overcoming the limitation of the additive range by minimizing the additive volume may be greater. To summarize, when the additive range is not large, such as a piercing punch, and the range of the mold strengthening is small, a method of processing and AM a mold part into a complicated shape may be disadvantageous in terms of cost. It is desirable to select the simplest shape to reduce the machining of the punch body and facilitate AM. For this purpose, it is necessary to develop a high-strength powder that can be deposited in a desired range (size) without any restrictions on the AM range (volume).

Alternatively, the results obtained from an analysis of the various semi-additive shapes presented to absorb the impact force acting on the punches became vulnerable to impact as the shape becomes more complicated. In addition, the phenomenon appearing in the analysis illustrates the stress is maximized at the beginning point of shearing, and the stress concentration was in the punch blade portion and the punch side surface. Additionally, the larger the additive area, the more susceptible to slipping or separating. Therefore, ensuring the side height of the punch is as low as possible in the semi-AM for punch strengthening may in-crease the life of the punch.

The semi-additive range and shape selected in this study was fabricated as a piercing semi-additive punch using the 3D printing AM DED technique as shown in Fig. 16 and the durability test was performed to verify the feasibility. The powder material of this semi-additive punch used the HWS of high wear-resistant tool steel, and the body (solid) material of the

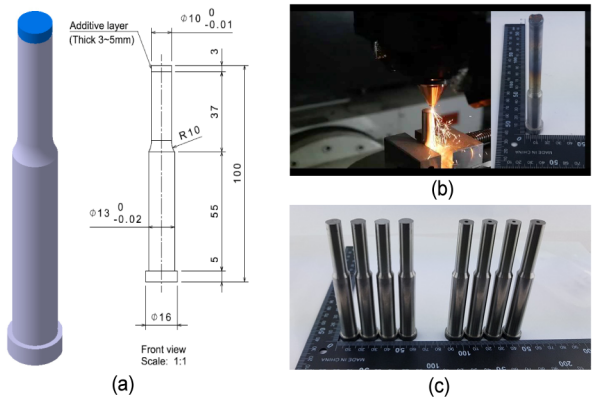

Fig. 16. Specification and manufacturing process of the semi-additive punch for the feasibility validation.

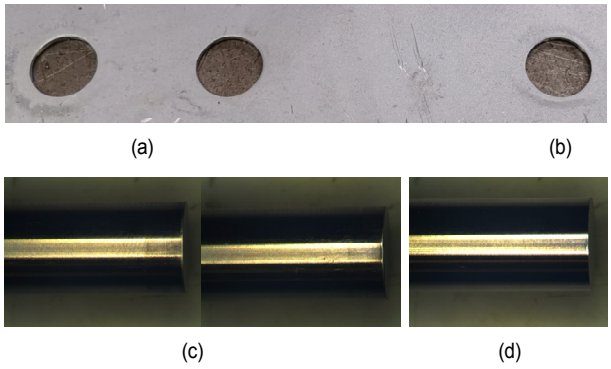

Fig. 17. Durability test results for feasibility validation of the semi-additive punch: (a) holes state by semi-additive punch; (b) hole state by solid punch; (c) semi-additive punch (HWS); (d) solid punch (SKD 11).

punch was SKD11 (D2). The metal 3D printer used I company's MX3 equipment of Korea. The durability test material for the feasibility verification was a CR980 sheet. The specifications for the semi-additive punch used for feasibility verification is shown in Fig. 16(a). The manufacturing process of the semi-additive punch by metal 3D printing AM DED technology is shown in Fig. 16(b).

The semi-additive punch was subject to a heat treatment and post-processing as shown in Fig. 16(c).

Fig. 17(a) shows the sample hole state of the sheet material after the durability test by the semi-additive punch, and (b) shows the sample holes state of the sheet material after the durability test by the solid punch. The piercing hole state of the sheet material by two kinds of punches is very good. Fig. 17(c) shows the SEM image of the semi-additive punch photographed after 1000 piercing processes, (d) shows the SEM image of the SKD11 solid punch photographed after 1000 piercing processes. The condition for punches of both types was very good. From this validation test, the feasibility of the semi-additive punch was confirmed by showing a similar state of scratches and abrasion from the two punches. Therefore, future research could include AM of cutting and trimming punch molds, punch manufacturing in special fields where high strength is required, regeneration and maintenance of punch molds discarded after a certain period of use, reduction of expensive powder materials, and reducing the AM time (which complements the low productivity of 3D printer AM technology and the high manufacturing cost).

8. Conclusions

In this study, simulation analysis was performed to choose the best shape for the semi-AM method as a strengthening method for the piercing punch. As a preliminary process, the punch strength required for the piercing process of high-strength sheet material was estimated through the process simulation based on the process variables. The range of the punch shape affecting the shear action were analyzed and measured from the simulation results of the punch strength. The semi-AM volume was defined based on the measured height and depth of the punch shape, and various semi-AM shapes were designed. The simulation analysis for the semi-additive shape verification was performed using the friction characteristics of the interface boundary condition for the designed semi-additive shape. The following results were obtained from the simulation analysis for the semi-AM shapes (geometry) used for strengthening a piercing punch:

1) The main factor affecting the punch stress prediction in the piercing process is the sheet material strength, while the effect of the punch material and punch speed (above a certain level) were insignificant.

2) The average maximum stress acting on the punch in the piercing process of the 22MnB5 high-strength sheet material was 3267 MPa, and the depth and height of the concentrated stress-producing punches were 1.3 mm and 3.2 mm, respectively.

3) The average maximum stress acting on the punch in the piercing process of CP1180 high-strength sheet material was 2256 MPa, and the depth and height of the concentrated stress-producing punches were 1.21 mm and 2.625 mm, respectively.

4) The semi-additive shape range (depth/height) predicted in this study was within 2-3 mm, which is a possible range for the AM of high-strength tool steel powder material by metal 3D printing.

5) A most stable geometry in the shape selection of this semi-AM was shown the horizontal flat type and the type having a triangular cross section. The bond interface was more stable in the case of having a 45-degree interface than the shape having a perpendicular and acute angle, or in the case of a pure straight line than the case of contains a curve.

6) In the case of a rectangular cross section with a vertical additive interface, the separation gross occurred as the interface moved away from the punch edge. Therefore, it is advantageous to prevent the separation phenomenon by depositing as a thin a layer as possible in the depth direction of the punch body.

7) In the shape selection of this semi-AM, the more compli-

cated AM shape is more vulnerable to impact, and the larger the manufacturing range, the more easily slip or separating occurs. Therefore, depositing thin and low layers in simple shapes as much as possible can improve the life of the semi-AM punch.

Acknowledgments

This research was supported by The Leading Human Resource Training Program of Regional Neo Industry through the National Research Foundation of Korea funded by the Ministry of Science, ICT and future Planning (2016H1D5A1910621).

References

[1] Z. Wang, H. Kubota, D. Xue, Q. Lin and M. Okamura, Galling behavior in square cup drawing of high-tensile-strength steel, *J. Jpn. Soc. Technol. Plast.*, 47 (549) (2006) 988-992.

[2] H. S. Choi, S. G. Kim, B. M. Kim and D. C. Ko, Quantitative evaluation of scratch related tool life for stamping of UHSS using pin-on-flat surface test, *Transactions of Materials Processing*, 22 (2) (2013) 86-92.

[3] G. Y. Baek, D. S. Shim, J. S. Seo and M. H. Kim, Hardfacing of Piercing mold using DED technique, *Conference of The Korean Society For Technology of Plasticity* (2016) 122.

[4] Y. S. Kim, R. Li, V. T. Hoang, J. W. Kum, Y. J. Yum and S. Y. Yang, A study on the production of full-additive manufacturing punch fabricated of high-strength mold steel powder materials using 3DP technique, *21st International Conference on Mechatronics Technology* (2017) 366-371.

[5] Y. S. Kim, R. Li, V. T. Hoang, J. W. Kum, Y. J. Yum and S. Y. Yang, A study on mechanical properties of HWS (high wear resistance steel) powder material using the additive manufacturing (AM) DED (directed energy deposition) process by metal 3D printing, *The 13th International Forum on Strategic Technology* (2018) 22.

[6] E. M. Lee, G. W. Shin, K. Y. Lee, H. S. Yoon and D. S. Shim, Study of high speed steel AISI M4 powder deposition using direct energy deposition process, *The Korean Society For Technology of Plasticity, Transactions of Materials Processing*, 25 (6) (2016) 353-358.

[7] G. Y. Baek, G. Y. Shin, E. M. Lee, D. S. Shim, K. Y. Lee, H. S. Yoon and M. H. Kim, Mechanical characteristics of a tool steel layer deposited by using direct energy deposition, *Metals and Materials International*, 23 (4) (2017) 770-777.

[8] D. S. Shim, G. Y. Baek and E. M. Lee, Effect of substrate preheating by induction heater on direct energy deposition of AISI M4 powder, *Materials Science & Engineering A*, 682 (2017) 550-562.

[9] E. M. Lee, G. Y. Shin, H. S. Yoon and D. S. Shim, Study of the effects of process parameters on deposited single track of M4 powder based direct energy deposition, *Journal of Mechanical Science and Technology*, 31 (7) (2017) 3411-3418.

[10] R. Li, V. T. Hoang, Y. S. Kim, Y. J. Yum, S. Y. Yang and J. W. Kim, A study on analytical prediction of punch strength required for ultra high strength parts in piercing process after hot stamping, *12th International Forum on Strategic Technology* (2017) 71.

[11] R. Li, V. T. Hoang, J. W. Kim, Y. S. Kim, Y. J. Yum and S. Y. Yang, A study prediction of punch shape range for improving punch strength by partial semi-additive method using metal 3D printing technique, *21st International Conference on Mechatronics Technology* (2017) 350-354.

[12] R. Li, V. T. Hoang, J. W. Kim, Y. S. Kim, Y. J. Yum and S. Y. Yang, A study on the semi-additive shape design for strengthening metal molds of functional part by using high alloy tool steel (high speed steel) powder and metal 3D printing technique, *2017 KSAE Annual Autumn Conference and Exhibition* (2017) 119.

[13] S. L. Wang, R. Li, V. T. Hoang, W. J. Kim, Y. S. Kim, Y. J. Yum and S. Y. Yang, A study on the optimization of punch edges shape for enhancing functional part of piercing punch, *Proceedings of the KSME Spring Annual Meeting* (2018).

[14] M. Shirgaokar, H. Cho and T. Altan, *New Developments in FEM based Process Simulation to Predict and Eliminate Material Failure in Cold Extrusion, Engineering Research Center for Net Shape Manufacturing (ERC/NSM)*, The Ohio State University, 339 Baker Systems, 1971 Neil Avenue, Columbus, Ohio, USA.

[15] H. K Kim and M. Yamanaka, Prediction and elimination of ductile fracture in cold forgings using FEM simulation, *SFTC REF #103*, Engineering Research Center for Net shape Manufacturing, Columbus, Ohio, USA.

[16] D. Y Kim, H. I. Park, J. W. Lee, J. H. Kim, M. G. Lee and Y. S. Lee, Experimental study on forming behavior of high-strength steel sheets under electromagnetic pressure, *Proc. IMechE Part B: Journal Engineering Manufacture*, 229 (4) (2015) 670-681.

[17] S. H. Cha, M. S. Ahn, J. D. Nam, P. K. Seo, K. W. Won and B. M. Kim, Development of the trimming die for the automotive sill side part with advanced high strength steel of CP1180, *The Korean Society for Technology of Plasticity 2012 Fall Conference* (2012) 211-214.

[18] H. S. Choi, J. W. Lee, S. G. Kim, D. C. Ko, P. K. Seo and B. M. Kim, The effect of process parameters on the characteristic of sheared edge in trimming of DP980, *The Korean Society for Technology of Plasticity 2012 Fall Conference* (2012) 542-545.

[19] A. Bardelcik, High strain rate behaviour of hot formed boron steel with tailored properties, *Mechanical and Mechatronics Engineering Theses*, University of Waterloo (2013).

[20] H. S. Choi, B. M. Kim, D. H. Kim and D. C. Ko, Application of mechanical trimming to hot stamped 22MnB5 parts for energy saving, *International Journal of Precision Engineering and Manufacturing*, 15 (6) (2014) 1087-1093.

[21] X. Wu and H. Bahmanpour, Characterization of mechanically sheared edges of dual phase steels, *Journal of Materials Processing Technology*, 212 (2012) 1209-1224.

[22] H.-W. Lee, J.-B. Hwang, S.-U. Kim, W.-H. Kim, S.-J. Yoo, H.-W. Lim and Y.-J. Yum, Construction of vehicle door impact beam using hot stamping technology, *The Transactions of the*

Korean Society of Mechanical Engineers A, 34 (6) (2010) 797-803.
[23] A. Yanagida and A. Azushima, Evaluation of coefficients of friction in hot stamping by hot flat drawing test, *CIRP Annals-Manufacturing Technology*, 58 (1) (2009) 247-250.
[24] B. Shapiro, Using ls-dyna for hot stamping, *7th European LS-DYNA Conference*, Stuttgart, Germany (2009).
[25] S. H. Cha, M. S. Ahn, J. D. Nam, P. K. Seo, K. W. Won and B. M. Kim, Development of the trimming die for the automotive sill side part with advanced high strength steel of CP1180, *The Korean Society for Technology of Plasticity 2012 Fall Conference* (2012) 211-214.
[26] H. S. Choi, J. W. Lee, S. G. Kim, D. C. Ko, P. K. Seo and B. M. Kim, The effect of process parameters on the characteristic of sheared edge in trimming of DP980, *Proceedings of the Korean Society for Technology of Plasticity* (2012) 542-545.
[27] A. J. Smith, Procedure and results for constitutive equations for advanced high strength steels incorporating strain, strain rate, and temperature, *Thesis for the Master Degree of Science*, The Graduate School, The Ohio State University (2012) 10-34.

Gaoqi Zhang is a master student of the University of Ulsan, Ulsan, Korea. He received his B.S. degree in Automotive Engineering from Kookmin University. His research interests include metal 3D printing technology, and simulation, dynamics, CAD, CAE.

Shiliang Wang is a researcher at Institute of Turbine and Propulsion Systems of Zhejiang University, Hangzhou, China. He received his M.S. in Mechanical Engineering from University of Ulsan. His research interests include metal 3D printing technology, and simulation, dynamics, CAD, CAE.

Yong-Seok Kim is a Research Professor of the School of Mechanical Engineering, University of Ulsan, Ulsan, Korea. He received his Ph.D. in Mechanical Engineering from University of Ulsan. His research interests include Metal 3D printing technology, mechanism design and simulation, dynamics, CAD, CAE.

Seong-Woong Choi is a Ph.D. of the Department of Construction Machinery Engineering, University of Ulsan, Ulsan, Korea. He received his M.S. in Mechanical Engineering from University of Ulsan. His research interests include future construction machinery, dual arm field robot, metal 3D printing technology.

Young-Jin Yum is a Professor of the School of Mechanical Engineering, University of Ulsan, Ulsan, Korea. He received his Ph.D. in Aeronautical Engineering from the Korea Advanced Institute of Science and Technology. His research interests include composite material, Metal 3D printing material.

Soon-Yong Yang is a Professor of the School of Mechanical Engineering, University of Ulsan, Ulsan, Korea. He received his Ph.D. in Mechatronics Engineering from University of Tokyo. His research interests include vehicle mechatronics, field robot, silver robot, metal 3D printing technology.